Experimental Study of Non-Newtonian Behavior of Foam Flow in Highly Permeable Porous Media

Sagyn Omirbekov, Hossein Davarzani, Azita Ahmadi-Senichault

Experimental study of non-Newtonian behavior of foam flow in highly permeable porous media

Sagyn Omirbekov[a,b], Hossein Davarzani*[,a], Azita Ahmadi-Senichault[b]

[a]*BRGM (French Geological Survey), 3 Avenue Claude Guillemin, 45100 Orléans, France*

[b]*Institut de Mécanique et Ingénierie de Bordeaux (I2M, TREFLE), Arts et Métiers ParisTech, 33405 Talence, France*

* Corresponding Author
Email address: h.davarzani@brgm.fr
Tel: + 33 (0) 2 38 64 33 52
Physical address: 3, avenue Claude Guillemin, 45100 Orléans, FRANCE

Abstract

Foam-flow behavior in highly permeable porous media is still unclear. Two types of pre-generated foam using porous columns respectively filled with fine sand and 1 mm glass beads were studied in different packs of glass beads with monodisperse bead size. Foam generated in fine sand had a sharp displacing front. However, the foam pre-generated using 1 mm glass beads had a transition zone front. We found that the transition foam-quality regime was independent of the porous medium grain size only when the bubbles are smaller than the pores. The apparent viscosity of foam was found to follow the Herschel-Bulkley model if the foam bubble sizes were smaller than the pore sizes. When the bubbles were the same size as the pores, the foam behaved like a Newtonian fluid at low flowrates and, by increasing flowrates, exhibited shear-thinning fluid behavior. Furthermore, the apparent foam viscosity was found to increase with permeability.

Keywords: foam flow, porous media, non-Newtonian fluid, yield stress, apparent viscosity

Highlights

- Bubble sizes affect apparent foam viscosity in high permeability porous media;
- Increasing of foam bubble size reduces the apparent foam viscosity;
- Liquid saturation in high permeability porous media changes with flow rate and foam quality;
- Transition foam quality is high and constant if bubbles size is smaller than pores size;
- Foam behaves as yield stress fluid in high permeability porous media.

1. Introduction

Foam is a two-phase system where gas bubbles are dispersed in a continuous liquid phase. The liquid phase in the foam is generally an aqueous solution containing a surfactant, which plays a crucial role in stabilizing the liquid films between bubbles.

Foam flow in porous media was firstly studied for a variety of applications in the production of petroleum and natural gas, especially in enhanced oil recovery (EOR). At the end of the last century, foam injection also started to be used as a soil remediation technique to remove non-aqueous phase liquids (NAPL) from aquifers (*1*). The primary use of foam in soil remediation operations is to control the permeability of porous media. By blocking highly permeable zones, foam injection allows remediation agents to be transported from high to low permeable zones in aquifers. Since the fraction of the surfactant used in foam injection is low, this is a better solution than surfactant flushing technology (*2*) from economic and environmental points of view. However, the differences in context between oil reservoirs and aquifers are significant. For instance, porous media in oil reservoirs are mainly low permeable and consolidated, while polluted aquifers are mostly unconsolidated and highly permeable. Oil reservoirs are subject to much higher pressure and temperature conditions than aquifers. Because of these differences, in situ foam generation in aquifers is questionable and successfully applying EOR models to highly permeable porous media is doubtful. Additionally, most studies presented in the literature concern low permeability media for EOR applications.

Our understanding of foam flow behavior in porous media is involved, due to the complex behavior of foam and apparent discrepancy in foam studies. For instance, Raza and Marsden (*3*) explored pre-generated fine-textured foam flow in four different Pyrex tubes, with radiuses varying from 0.25 to 1.50 mm. They noticed the non-Newtonian shear-thinning behavior of foam with foam quality from 70% to 96%. Moreover, foam at low flow rates exhibited a linear behavior while at high flow rates, a non-linear behavior was obtained. They pointed out an increase in the apparent foam viscosity with both tube radius and foam quality. Hirasaki and Lawson (*4*) experimentally measured the apparent viscosity of pre-generated foam in smooth capillaries and developed a mathematical model. They showed shear-thinning behavior in which the dependence of the apparent foam viscosity was proportional to -1/3 power of velocity. Falls et al. (*5*) extended these results by examining the apparent foam viscosity in homogenous bead packs, where they demonstrated the shear-thinning behavior of foam flow in porous media. They indicated that the apparent gas viscosity depends on foam bubble size in porous media. Several other authors have considered the existence of yield stress based on a threshold pressure gradient, which depends on the types of gas and surfactant, surfactant concentration, and petrophysical properties of porous media (*6*,*7*,*8*,*9*). Persoff et al. (*10*) studied foam flow through sandstone by co-injecting gas and surfactant solution at elevated pressure. They summarized foam flow in porous media as rheopectic, with Newtonian behavior for the liquid phase and pseudoplastic behavior for the gas flow, at steady state. Rossen (*11*) investigated the rheology of strong foam at steady state by limiting-capillary-pressure concept based on the working hypothesis of Persoff et al. (*10*) and Ettinger and Radke (*12*). He found that foam behaves as a Newtonian fluid in steady 1D radial flow in which capillary pressure is nearly constant at the value of "limiting capillary pressure," despite that foam with uniform texture behaves as a non-Newtonian fluid. He pointed out the necessity of a quantitative understanding of the mechanisms that control bubbles and rheology for designing foam processes. Moreover, he concluded that

the study of the relative permeability and yield stress fluid viscosity individually is debatable, since assumptions on relative permeability strongly affect the foam viscosity. Patzek and Koinis (*13*) showed foam's shear-thickening behavior in field cases where the apparent viscosity of steam foam was decayed as much as the foam flowed far from the injector wells. Based on the experimental results of Alvarez (*14*), Rossen and Wang (*15*) considered bubbles roughly the same size as pores in low-quality regimes, where bubbles smaller than the pore size were expected to grow rapidly to pore size due to gas diffusion between bubbles. As a result, they modeled foam with a fixed bubble size as a Bingham plastic. Vassenden and Holt (*16*) presented a model based on the relative permeability concept and validated it by experimental data. They demonstrated a transition of foam flow behavior from Newtonian to shear-thinning, according to increases in the gas flow rate. Alvarez et al. (*17*) conducted experimental studies in several types of sandstones and sands for which the permeability ranged from 0.3 to 3 Darcy. They pointed out the dependence of apparent foam rheology on foam quality (foam gas volume fraction, f_g) where foam flowed as a shear-thinning fluid in the low-quality regime and as a shear-thickening fluid in high-quality regimes. Furthermore, in previous studies, the yield stress behavior of stationary lamellae was studied on the pore-scale level (*5*,*18*,*19*,*20*). Some authors also considered yield stress as a fixed parameter depending on the ratio of surface tension to pore throat, considering the porous media as a bundle of capillary tubes (*21*,*22*). Others (*23*,*24*,*25*) presented foam in low permeability consolidated porous media as a yield stress fluid, which was also described by a threshold pressure (*26*). For example, Simjoo and Zitha (*25*) studied N_2 foam flow in a Bentheimer core in which foam was generated in situ using alpha-olefin sulfonate ($C_{14\text{-}16}$, AOS) surfactant in 0.5 M NaCl brine. The foam behavior with a quality of 91% was analyzed through X-ray Computed Tomography and the results of 6 pressure transducers along the 38.4 cm long core. They observed two foam displacement fronts: 1) the forward primary foam front which was characterized by a low mobility reduction factor (MRF, a ratio of measured pressure drop of foam flow to the corresponding pressure drop for water flow) and high overall liquid saturation (S_w); 2) the backward secondary front with high MRF and more moderate S_w. This phenomenon explained by the transition of foam from weak to strong state at a liquid saturation of S_w=0.25. They found that yield stress was nearly equal to zero for weak foam, and when S_w is lower than 0.25 (i.e., strong foam), yield stress increased significantly. Nevertheless, in most foam-modeling studies in porous media, foam was described as a pure power-law fluid without considering yield stress (*27*,*28*,*29*,*30*,*31*,*32*,*33*).

Recently, Osei-Bonsu et al. (*34*) studied pre-generated foams via two sintered glass discs (with the pores size distribution of 16-40 μm and 40-100 μm) to investigate the link among foam quality, apparent viscosity, bubble size and cell permeability in a 2D Hele-Shaw cell with dimensions of 31 × 20 × 0.6 cm. They showed increasing of foam viscosity with foam quality (between 81% and 99%), which was obtained with the fixed gas rate at 10 mL/min and varying the liquid flow rates. The independence of pressure drop from gas flow rate was assumed based on the outcomes of Osterloh and Jante (*35*), which commonly occurs in high-quality regimes. Moreover, they pointed out a decrease of apparent foam viscosity with increasing flow rate for qualities of 93% and 98%. Shojaei et al. (*36*) studied pre-generated foam using sintered glass discs (with the pores size distribution of 16-40 μm) like Osei-Bonsu et al. (*34*) injected in a Vosges sandstone fracture replica with a length of 26 cm and a width of 14.8 cm. The mechanical and hydraulic apertures were 0.86 mm and 0.5 mm, respectively. They examined the apparent viscosity as a function of foam quality with the same technique as Osei-Bonsu et al. (*34*). Moreover, the

foam with a foam quality of 85% was examined at different flow rates, and all results were compared with the findings of Osei-Bonsu et al. (*34*). They observed the shear-thinning behavior of foam with yield stress in which the power-law index was -0.41 compared to the index value of -0.27, found by Osei-Bonsu et al. (*34*) for the Hele-Shaw cell. They also observed a decrease of apparent foam viscosity with increasing foam quality that was contrary to the findings of Osei-Bonsu et al. (*34*). Nevertheless, they admitted that the rheology of bulk foam is not identical to the one observed in porous media.

Most of the studies we reviewed were performed on consolidated media with permeable porosity lower than soil remediation cases, either in capillary tubes or in Hele-Shaw cell at the pore-scale. To the best of our knowledge, the study of foam behavior in highly permeable aquifers is still lacking, mainly when pore size greatly exceeds the bubble size. Here, we studied foam behavior in high permeability porous media with a special focus on the impact of the foam bubble size and quality and the porous medium's permeability. Our goals were two-fold: to characterize the surfactant solution and the gas and to investigate the pre-generated foam flow's experimental behavior. We achieved this by investigating the rheology of foam flow depending on bubble and grain sizes (permeability) in a highly permeable unconsolidated porous medium, performing laboratory experiments in 1D columns.

2. Theoretical considerations

Three major foam generation mechanisms are identified at the pore-scale in porous media: snap-off, leave-behind, and lamella division (*37*). Depending on the generation processes, flow rate, permeability, compressibility, and the length of the system, foam may be classified as "weak" or "strong" (*8*,*38*), which can be described by a transition from weak continuous gas foam to strong discontinuous gas foam with a particular transition zone (see Fig. 1). Weak foam usually occurs through leave-behind processes, while strong foams are generated by all three mechanisms. As previous studies have stated (*6*,*7*,*8*,*9*,*18*), foam is generated when the pressure gradient exceeds a critical pressure gradient denoted ∇P^* (Fig. 1). This pressure gradient depends on a minimum capillary number for entry into pores by the snap-off mechanism.

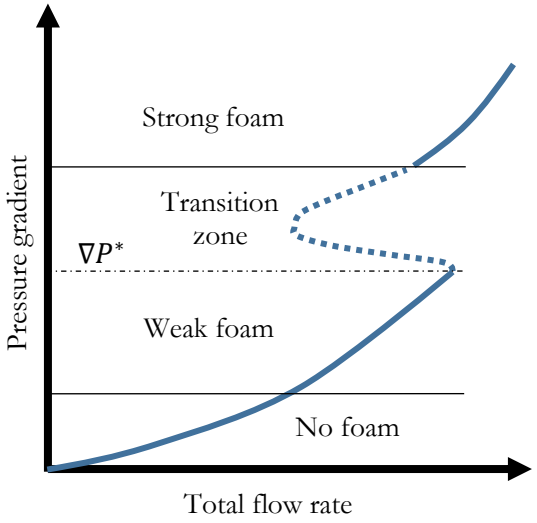

Fig. 1 Sketch of foam formation in porous media, adapted from (*39*)

Several authors (*6*,*7*,*8*,*40*) calculated the minimum capillary number to generate foam in porous media. By examining a variety of porous media, Tanzil et al. (*7*,*40*) calculated the minimum capillary number N_{cL}=2, with the capillary number N_{cL} defined as

$$N_{cL} = \frac{\Delta P}{\sigma}\sqrt{\frac{K}{\varphi}} \tag{1}$$

where σ (N/m) is gas-liquid interfacial tension, K (m²) is the permeability of the porous column, φ (-) is porosity, and ΔP (Pa) is the measured pressure drop along the column. ΔP depends on the foam quality, which is the ratio of the gas volume on the total volume, and can be written as

$$f_g = \frac{Q_G}{Q_G + Q_L} \tag{2}$$

where Q_G (mL/min) and Q_L (mL/min) are the volumetric gas and liquid flow rates, respectively. According to foam quality values, bulk foam can be dry (f_g>99%), wet (64%<f_g<99%), or considered as a bubbly liquid (f_g<64%) (*41*).

In porous media, Osterloh and Jante (*35*) identified two specific foam-flow regimes in steady-state flow in sandpack experiments, depending on foam quality. The permeability of the sandpack was 6.2 Darcy in which nitrogen and surfactant solutions were simultaneously injected, in order to study the behavior of the foam generated in situ. They observed a low-quality regime (wet), in which the pressure gradient was constant regardless of the liquid flow rate, and a high-quality regime (dry), in which the pressure gradient was independent of the gas flow rate. These two regimes were separated by a transition foam quality f_g^*, which depended on the porous media's characteristics, types of surfactants, and gas (*17*). When f_g was lower than f_g^*, foam flowed at the low-quality regime. If foam quality was higher than f_g^*, foam flowed at the high-quality regime. The existence of the transition foam quality became evident when the critical capillary pressure was reached, as that depends on foam stability in porous media. Foam flow in porous media is also affected by gravity. The competition between gravity and capillary forces may lead to different flow configurations. This competition is quantified by the Bond number, which is calculated using the following equation (*8*):

$$N_{Bo} = \frac{\Delta\rho g R_g D}{\sigma} \tag{3}$$

where $\Delta\rho$ (kg/m³) is the gas-liquid density difference, g (m/s²) is the gravitational acceleration, R_g (m) is the grain radius, D (m) is the porous column diameter, σ (N/m) is gas-liquid surface tension.

The model used in this work to fit the rheological behavior of foam is the Herschel-Bulkley (H-B) model (*42*) presented as follows:

$$\mu_{app}(\dot{\gamma}) = k\left|\dot{\gamma}_{eq}\right|^{n-1} + \frac{\tau_0}{\left|\dot{\gamma}_{eq}\right|} \tag{4}$$

where τ_0 (Pa) is the yield stress, k (kg/m.s) is the consistency index, n is the flow index. The Herschel-Bulkley flow index n controls the overall behavior of flow, where 0< n<1 for a shear-thinning fluid, n=1 corresponds to the Bingham fluid model (*15*), and n>1 gives a shear-thickening fluid.

3. Foam characterization

Since foam is a two-phase system affected by the fractions of gas and surfactant solution, the first step of the investigation was to choose the surfactant and the gas for foam-generation purposes. Careful selection of chemical surfactants was necessary, keeping in mind potential environmental effects, since some synthetic surfactants are toxic and less biodegradable.

3.1 Selection of a surfactant and the surfactant concentration

After considering several studies on chemical surfactants (*43*), taking account of biodegradability in soils (*44*,*45*,*46*), market accessibility (*47*), and field tests for soil remediation purposes (*48*), $C_{14\text{-}16}$ alpha-olefin sulfonate (AOS, Solvay Novecare) was chosen as the most suitable surfactant to generate foam. AOS is an anionic surfactant that is historically the oldest and most commonly used surfactant. It is gentle on the skin and is used in detergents, shampoos, and ordinary bath soaps. The surfactant used contained 40 wt% of active materials in an aqueous solution. To find its critical micelle concentration (CMC), surfactant solutions with different concentrations were examined through drop-shape analyzer (DSA-100S, KRUSS). The surfactant solution was prepared by using demineralized/degassed water. The measurements were conducted by the pendant drop method (*49*). The results are presented in Fig. 2. We found that the CMC and the corresponding surface tension were 1.8±0.1 g/L and 36±1 mN/m, respectively.

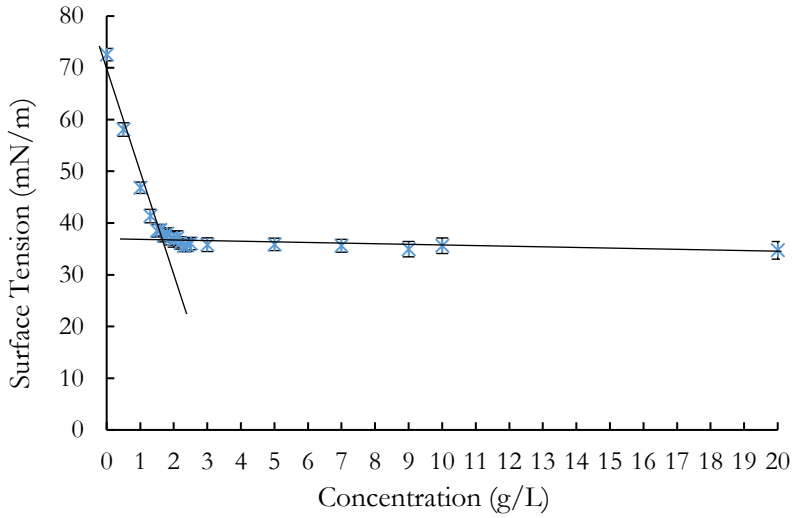

Fig. 2 Surface tension as a function of surfactant concentration

We also carried out foam stability experiments using a dynamic foam analyzer (DFA-100, KRUSS) to find the best surfactant concentration for foam formation in terms of stability and foamability. We analyzed the stability of bulk foams generated with different surfactant concentrations (multiples of CMC) by measuring the half-life time and also the foamability. Gaseous nitrogen with 99.98% purity (Air Liquide) was used to generate bulk foam. The investigation methodology we adopted followed Yoon et al. (*50*). The results of the test presented in Fig. 3 show

an increase of foam stability (half-life time) until the concentration of two times CMC that corresponds to the maximum value of half-life time. This phenomenon, i.e. the increasing of foam stability with surfactant concentration, was also observed in previous studies (*51*,*52*,*53*). However, the values of half-life time dropped after 2 × CMC and were almost constant when surfactant concentration increased further. This means that an optimum concentration exists, which corresponds to the maximum foam stability. This fact can also be confirmed by the results of Farzaneh and Sohrabi (*54*), in which they pointed out the presence of an optimum surfactant concentration for some surfactants in terms of stability. The foamability results also demonstrated increasing behavior with concentration up to the highest value of foamability, which was obtained at three times CMC. Nevertheless, it decreased sharply and followed the trend of half-life time results for higher values of concentration. Consequently, we observed that the dependence of foam stability and foamability on CMC is rather similar. The decrease in foamability at high concentrations can be explained by the achievement of surfactant solubility (*55*).

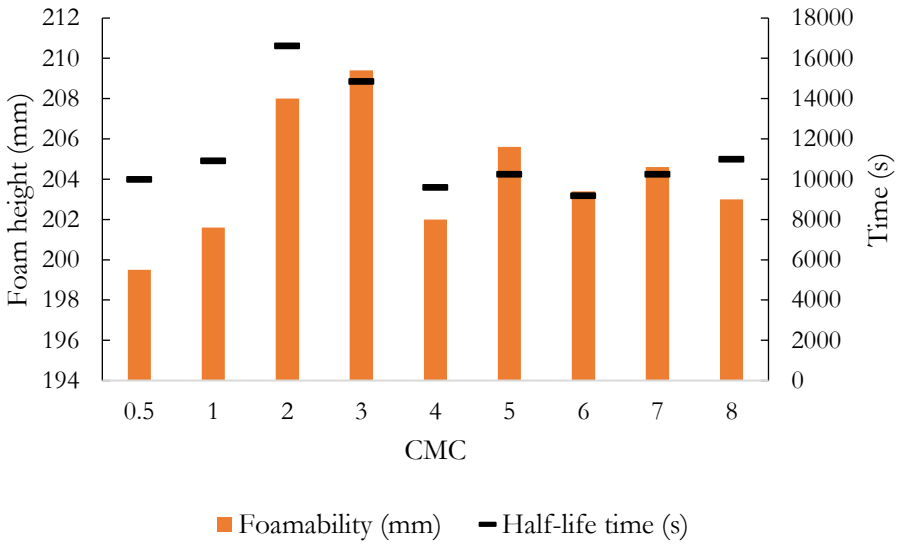

Fig. 3 Foam stability and foamability measurements as a function of concentration as multiples of CMC

Foamability, stability, and adsorption issues in the presence of oil have been studied in the literature (*56*). However, a thorough review of these studies is beyond the scope of this paper, where foam is never in contact with oil. The surfactant concentration was chosen to be four times CMC with a margin to ensure not only stability and foamability but also high surfactant concentration in case of adsorption (*57*) processes in soil (*58*), although high surfactant concentration may tend to delay the biodegradability process, which is important from the point of view of environmental use.

3.2 Gas selection

Gas is the second principal component of foam. We investigated 99.98% pure N_2 and CO_2 gases (Air Liquide) to select the gas for further experiments. We examined stability and foamability using the DFA-100 foam analyzer, where the concentration of the surfactant solution was taken equal to 4 × CMC. The methodology was the same as previous experiments (*50*). Fig. 4 shows the results of bulk foam experiments in terms of half-life time and

foamability for CO_2 and N_2 gases. Foam generated using N_2 is more stable and has higher foamability than CO_2 foam.

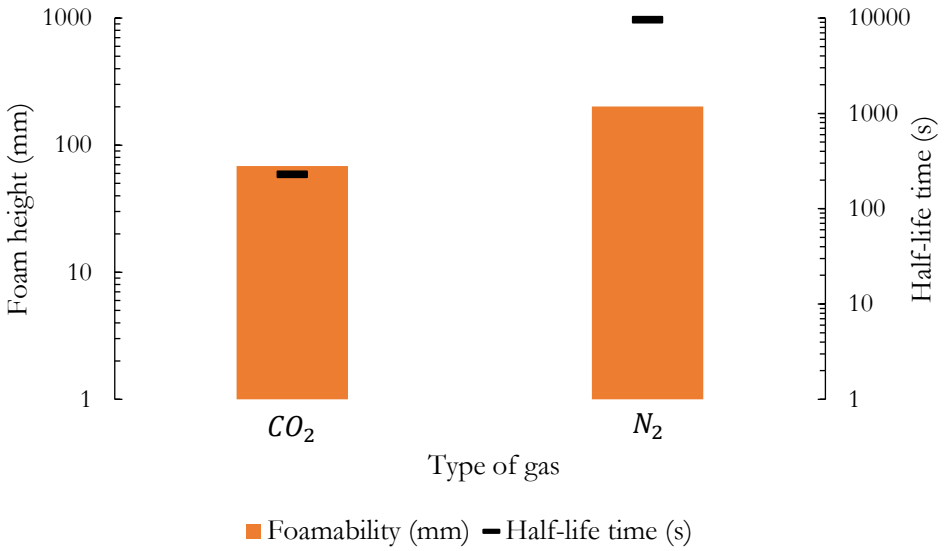

Fig. 4 Foam stability and foamability of CO_2 and N_2 gases

Since CO_2 is about 55 times more soluble in water than N_2 gas (*59*), the foam generated using N_2 is much more stable, as confirmed by the work of Farajzadeh et al. (*60*). As a result, we chose N_2 gas for the next experiments.

4. Experimental details

4.1 Materials

The characterization presented in the previous section demonstrated the consequences of the choices of surfactant and gas used for foam generation. AOS with a concentration of 4 × CMC and N_2 gas were selected for the next experiments. The porous media considered here were unconsolidated, homogenous packings of calibrated glass beads (GB), and quasi-homogeneous silica sand (BR37), provided by Sigma-Aldric and Sibelco, respectively. The grading characteristics of the sand were as follow: the uniformity coefficient (Cu) and the curvature coefficient (Cc) were 0.72 and 0.98, respectively; the effective size (d_{10}) and mean grain size (d_{50}) were 0.180 mm and 0.135 mm, respectively. The measured properties of all porous media are presented in Table 1. Unlike natural soil, porous media made by packing of glass beads prevent adsorption and ensure homogeneous pore distributions. By testing various sizes of calibrated GB, we analyzed the effect of porous media grain size and consequently pore size, bubble size, or permeability on the foam's rheological behavior.

Table 1 Properties of porous columns (Porous Media)

Porous media	Mean grain size diameter, d (mm)	Porosity, φ (%)	Permeability, K (D)	Pore Volume, PV (mL)	Mean pore radius, r_p (µm)
Sand BR37	0.135	38±1	7±1	51±2	11.5
GB 1	1	36±1	830±10	181±2	133.5
GB 2	2	35±1	3017±10	181±2	257.9
GB 4	4	40±1	11032±10	185±2	467.2
GB 8	8	41±1	41125±10	191±2	886.4

The porosity of the medium was determined by measuring the mass of the main column before and after the water saturation processes. The permeability was calculated by relating measured values of the pressure difference for different water flow rates to the corresponding imposed flow rates through Darcy's law given by (*61*):

$$u = \frac{Q}{S} = -\frac{\boldsymbol{K}}{\mu}.\nabla P \tag{5}$$

where $\boldsymbol{K}$ (m²) is the intrinsic permeability tensor ($\boldsymbol{K} = K\boldsymbol{I}$ for an isotropic porous medium), μ (Pa.s) is the dynamic viscosity of the fluid, ∇P (Pa/m) is the pressure gradient linearly dependent on Darcy velocity u (m/s). Q and S correspond respectively to the flow rate and the cross-section surface of the sample. The mean pore radiuses were calculated using the following equation proposed by Kozeny (*62*), which was derived from Darcy's equation (Eq. 5) and Poiseulle's law (*63*) using a model porous medium composed of a bundle of parallel capillaries of identical radius r_p.

$$r_p = \sqrt{\frac{8K}{\varphi}} \tag{6}$$

In the preceding equation, r_p (m) is considered as the mean pore radius. K (m²) and φ (-) are the intrinsic permeability and porosity of the porous medium, respectively.

4.2 Experimental setup

The setup used to conduct the foam flow experiments is shown in Fig. 5. In this setup, N_2 and AOS-based surfactant solutions were co-injected into the foam-generator column to generate foam. Then the foam was injected into the main column packed with glass beads of the different sizes (Table 1).

An El-Flow Select F-201CV mass flow controller (Bronkhorst) 0.16-10 mL_n/min (±0.5 % reading plus ±0.1 % full scale) was used to ensure stability in the gas flow and control the flow rate from the gas bottle. A DCP50 dual cylinder positive displacement pump (Strata) with ±1.5 % setting accuracy was used to inject the surfactant solution at a constant flow rate. The setup consisted of two porous columns, the first "foam generator" (FG) and the second "main" (M) made of transparent PVC (polyvinyl chloride) tubes 10 cm and 40 cm long, respectively. The inner diameter of the columns was 4 cm. A Rosemount 2051 differential pressure transmitter (Emerson), with a range 0-623 mbar (±0.666 mbar at the maximum value) or 0-2500 mbar (±7 mbar at the maximum value), was used to measure the pressure drop along the main column. The mass of the effluent was measured by a STX 6201

electronic balance model (OHAUS) with a minimum of 0.1 g readability. The maximum pressure limit of the experimental setup was six bars, which was controlled by the pump's pressure sensor.

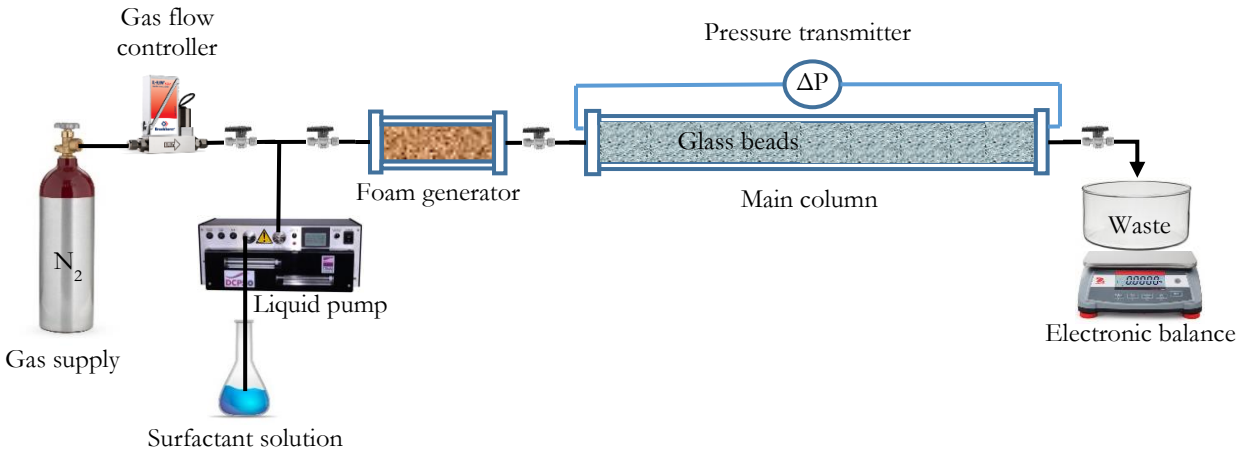

Fig. 5 Schematic of the experimental setup used to conduct foam flow experiments

Two different foam generators were used. The first pre-generator column was packed with BR37 fine sand, and metallic grids with 42 μm cell size were used to curb the porous media. The second generator column was prepared using 1 mm glass beads. Glass beads with the diameters being tested (d=1, 2, 4, and 8 mm) were used to pack the main column, and metallic grids with 150 μm cell size were used to hold all the glass bead packings. The same foam generator column was used during all the experimental procedures. However, a new main column was prepared for each experimental cycle corresponding to a different bead size.

4.3 Experimental procedure

After packing both columns and checking for leakage, the columns were flushed with CO_2 gas to remove air from the porous samples. Then the columns were saturated with degassed, demineralized water in a vertical position with a 5 mL/min flow rate to dissolve any CO_2 and saturate the columns thoroughly without trapping the gas. In total, around three pore volumes (PV) of demineralized/degassed water were injected. Columns were weighed before and after the water saturation step to measure the pore volume and porosity. The permeability measurements were carried out by injecting demineralized, degassed water with different flow rates, and measuring the pressure differences. Permeability was calculated using Darcy's law (Eq. 5). To satisfy the porous medium's surfactant adsorption capacity (*25*), the columns were flushed with 3 PV of surfactant solution. The permeability and porosity of the generator column (fine sand) were rechecked. After checking the porous media parameters, the surfactant solution and the nitrogen gas were co-injected into the generator column to produce foam. 5 PV of fluids were co-injected to obtain a stable foam from the pre-generator, which was chosen considering the work of Simjoo and Zitha (*25*). The total flow rate (Q_t=$Q_G + Q_L$) was increased step by step from the minimum (0.2 mL/min) to the maximum (3 mL/min) technically possible values. The proportion of liquid/gas was adjusted simultaneously for each value of the total flow rate (Q_t) in order to keep the foam quality constant. The stabilization time for each experimental cycle was 7 PV. Each experiment was duplicated by at least one descending flow rate experiment. The foam flow experiments were analyzed using the flow rate and pressure drop measurements along the column. The liquid effluent mass was measured using an electronic balance to determine the change of

surfactant solution saturation inside the main column (S_w). In addition, each porous column was weighed after the first drainage to establish the initial surfactant solution saturation (S_{wi}).

4.4 Strategy

First, all the porous media were studied to find the transition (f_g^*) between the two foam flow regimes (low and high-quality regimes) where foam flow behavior was examined at a fixed total flow rate (2 mL/min) by varying the foam quality. The goal of this experiment was to define the transition zone, which would prevent instability during the rheological studies. After determining f_g^*, the rheology of foam in porous media (confined foam) was studied at a given foam quality. Table 2 shows the experimental conditions for all the rheological studies. Next, to see the effect of bubble size on foam viscosity, the rheology of two different foams generated through the packing of fine sand and 1 mm GB generators were studied in the main column filled with 1 mm GB at f_g=85%. Note that the foam bubbles were considered to be the same size as the pores of the generator column, according to the model of Rossen and Wang (*21*).

Finally, the foam generated using the generator column was investigated in four types of glass bead packings at a fixed f_g=85% by varying the total flow rate (0.2 – 3 mL/min). The main idea was to study how foam rheology depends on grain size, and consequently pore size. We analyzed the apparent foam viscosity μ_{app} given by the following equation (Eq. 7) that was obtained from the main column using Darcy's law (Eq. 5) and fitted it to a rheological model of a yield stress fluid.

$$\mu_{app} = \frac{K\Delta P}{uL} \tag{7}$$

Table 2 Experimental conditions

Foam generator material	Main column material	Foam quality (f_g)
Sand BR37	GB 1	85%
	GB 2	85%
	GB 4	85%
	GB 8	85%
GB 1	GB 1	85%

5. Results and Discussion

5.1 Foam generation in highly permeable porous media

In situ foam generations (gas and surfactant co-injection) in the foam generator column after the injection of 0.6 PV are shown in Fig. 6, for different soil types and flow rates. Fig. 6a shows the process during the first drainage experiment in the foam generator column filled with fine sand, where the total flow rate was equal to 2 mL/min. The piston-like displacement of foam in the porous pre-generator was observed with a vertical transition zone.

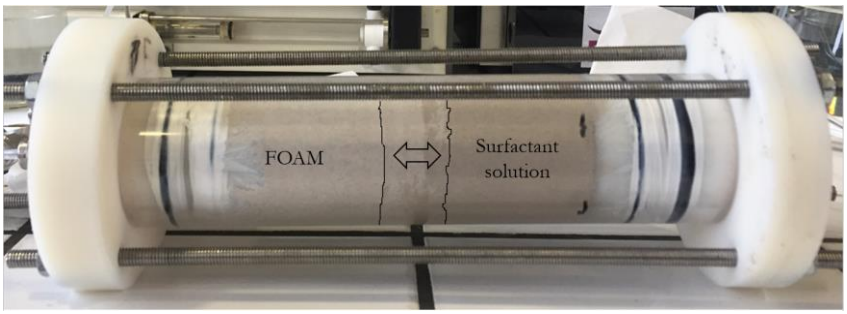

a)

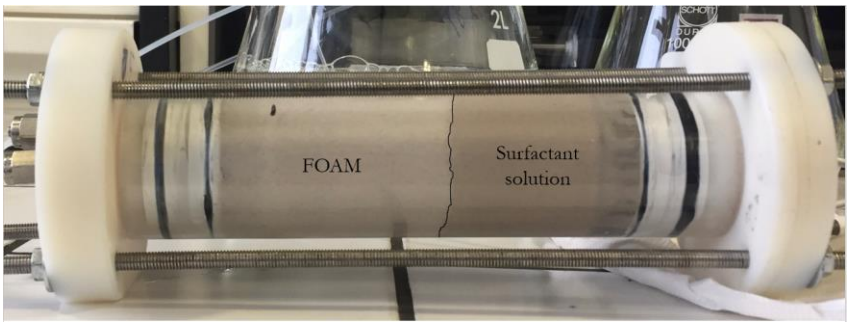

b)

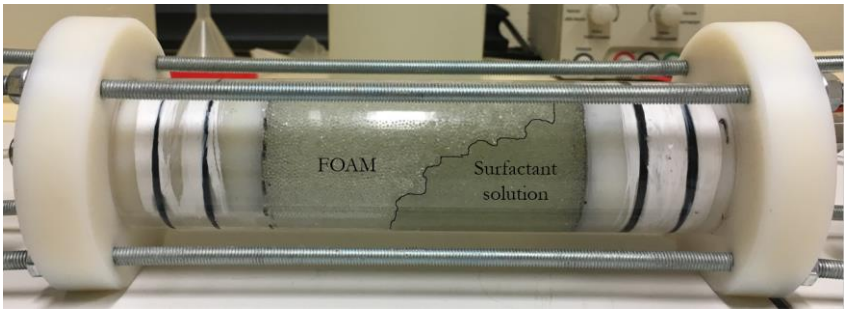

c)

Fig. 6 In situ foam generation in foam generator column (after 0.6 PV injection):

a) sand BR37, at Q_t=2 mL/min, b) sand BR37, at Q_t=8 mL/min, and c) 1 mm glass beads, at Q_t = 2 mL/min

This transition zone occurs due to the transition from "weak foam" to "strong foam," which is explained by the foam generation process in porous media (see Fig. 1). At this total flow rate, the foam generation mechanism is called "snap-off" and depends on local dynamic capillary pressure. However, when the total flow rate increases further, the pressure drop jumps abruptly to much higher values due to foam generation mechanisms in porous media. Hence, the generation of strong foam requires a high-pressure gradient or depends on injection rates where the "lamella division" mechanism can play a crucial role. The lamella division mechanism concerns foam lamella that already exist and increases the number of bubbles. For this, it is necessary that the static lamellae in the pore throats be displaced by a sufficient pressure gradient. To check this fact, we conducted another drainage experiment by increasing the Q_t. In this experiment (see Fig. 6b), the total flow rate was four times higher (8 mL/min) than the previous one, and no transition zone was observed (pure piston-like displacement). Nevertheless, during the experiment, the pressure gradient increased strongly, and we were forced to stop the experiment due to the pressure limitation of the experimental setup. After that we carried out the co-injection

process at Q_t=2 mL/min in the foam generator column packed by 1 mm glass beads. The drainage of the surfactant solution at 0.6 PV is presented in Fig. 6c. The border between the foam and the saturated zone is shown clearly to have a given slope due to the weak foam and gravity effects. Indeed, the Bond number (Eq. 3) was nearly ten times larger for the porous pre-generator made by the packing of 1 mm glass beads vs the one made by sand. Once the foam generation processes in porous media were analyzed, the pre-generated foam was injected into the main column. Fig. 7 shows the front of the foam flow in the main columns packed with 1 mm glass beads, where the foam was pre-generated in the fine sand (a) and in the 1 mm glass beads packing (b), respectively.

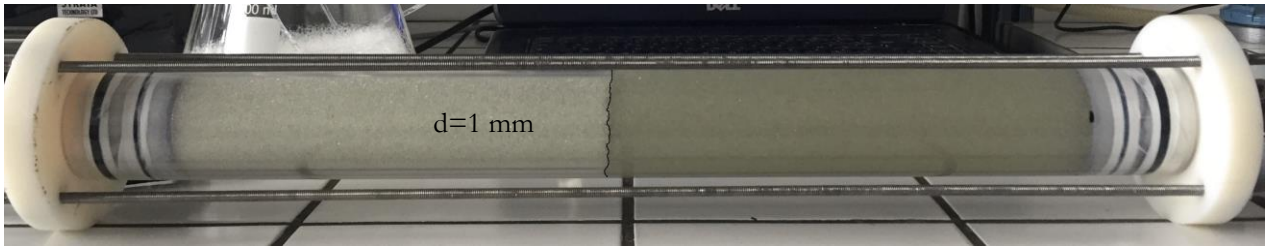

a)

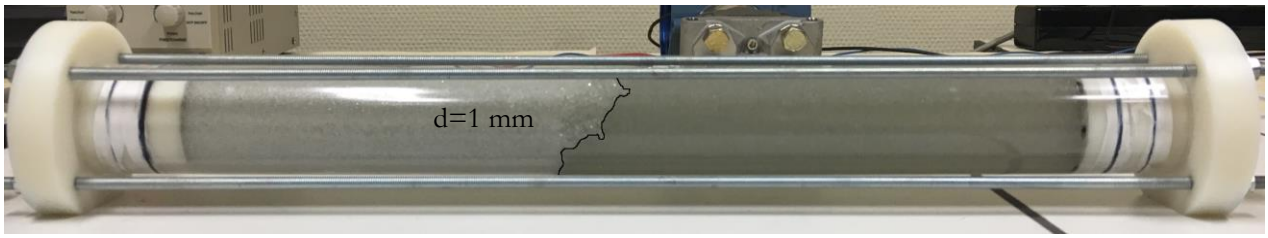

b)

Fig. 7 Injection of the pre-generated foam in the main columns at Q_t=2 mL/min: foam generated a) in the fine sand b) in 1 mm glass beads (t=0.5 PV)

If we visually compare the two columns, foam generated in fine sand features strong foam behavior, which has a sharp displacing front. However, the foam produced using 1 mm glass bead pre-generator has a transition zone with a particular slope, which could be explained by the presence of weak foam at the interface. These circumstances occurred when the pressure drop was lower than ∇P^*in the interface; hence, the weak foam was formed. Since all experimental conditions were identical except for the pre-generator columns, the values of capillary and Bond numbers and the bubble size may explain this phenomenon.

Fig. 8 shows the values of capillary and Bond numbers for different foam-generator and main-column systems, which were calculated at the steady-state. Since the value of the Bond number is the same and exceeds one (N_{Bo}=10.9), the capillary forces are small in relation to gravity forces. However, the values of the capillary number in the main column, for Q_t=2 mL/min, were 94 and 79.9 for the foam generated by sand and 1 mm glass beads, respectively. Whereas, the mean size of the bubble in the sand foam generator was 11 times smaller than foam made in 1 mm glass beads if we assume that the bubbles were roughly the same size as the pores (see Table 1). Therefore, the foam produced using a sand generator was more viscous, and we can confirm that the variation of foam viscosity depends on the bubble size. In addition, several authors experimentally showed that apparent foam viscosity has strong dependence on the texture or bubble size at the pore scale (*4*,*64*,*65*,*66*,*67*). Since most of the investigations carried out were for applications in the oil industry, where pore sizes are much smaller than in

aquifers, bubble sizes have been considered to be roughly equal to pore size due to the coarsening of small bubbles because of gas diffusion. However, note that coarsening of bubbles in aquifers needs much more time because of large pore sizes.

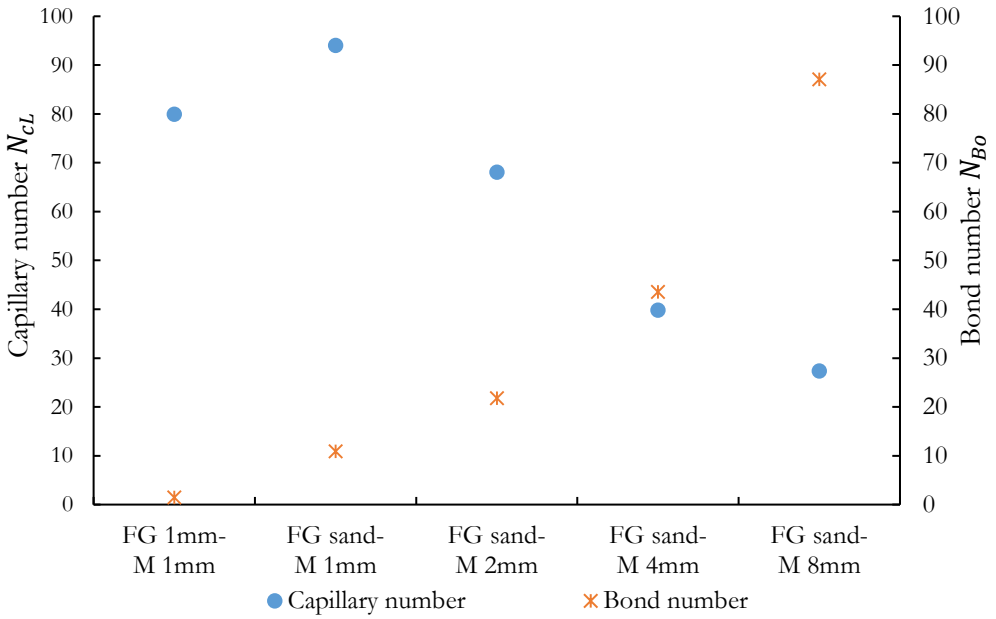

Fig. 8 Capillary and Bond numbers for different foam generators and main columns (f_g=85%, Q_t=2 mL/min)

As mentioned above, pre-generated foam in the fine sand was also studied in 2 mm, 4 mm and 8 mm glass beads packings. The same behavior as in 1 mm glass beads packing was observed in the column packed with 2 mm glass beads. However, with 4 mm glass beads, we observed a foam front with a particular inclination. This slope at the foam front was even more significant in 8 mm glass beads (data not shown). These phenomena can be explained by increasing gravity forces with the grain size. As is shown in Fig. 8, values of Bond number are more critical than capillary numbers for 4 and 8 mm glass beads. We conclude that gravity forces become more dominant than combined viscosity and surface forces.

Additionally, after the first drainage experiment, we determined the initial saturation (S_{wi}) of the surfactant solution for each porous column (Table 3). The S_{wi} increased with grain size. Since foam gravity forces were more important with the 4 and 8 mm glass beads (see Fig. 8), the effect of gravity-driven drainage increased the liquid saturation of porous media when the pore sizes became larger. We also observed the dependence of S_{wi} on the foam generator (bubble size), which increased with bubble size.

Table 3 Initial surfactant solution saturation after the first drainage (f_g=85%, Q_t=2 mL/min)

Foam generator	Main column	S_{wi} (%)
Sand BR37	GB 1	2.82
	GB 2	2.99
	GB 4	4.10
	GB 8	5.58
GB 1	GB 1	4.10

The previous analysis of the mass balance using measurements of the effluent mass as a function of time did not lead to notable differences in production mass for various flow rates. Therefore, we tested an alternative procedure to measure S_w only for the 1 mm GB packed pre-generator and main column. The mass of the main column was measured after each experiment by simultaneously closing the inlet and outlet tubes. Fig. 9a shows the saturation of the surfactant solution as a function of the total flow rate. No particular trend on the change of S_w with Q_t was observed, and the average S_w was equal to 4.5%±1.2%. However, a decrease in S_w was observed below 1 mL/min, followed by a slight increase and stabilization above 2 mL/min. Therefore, liquid saturation cannot be considered independent of the flow rate in high permeability porous media, which is contrary to the findings of Ettinger and Radke (*12*) and others (*10*). Those studies were carried out comparatively in low permeability sandstones and the saturation was found to be 30-40% regardless of the foam quality. However, Fig. 9b shows the linear decrease of S_w with increasing of foam quality that we observed, and that is trivial due to the reduction of the liquid fraction. Hence, in highly permeable porous media, S_w falls with foam quality.

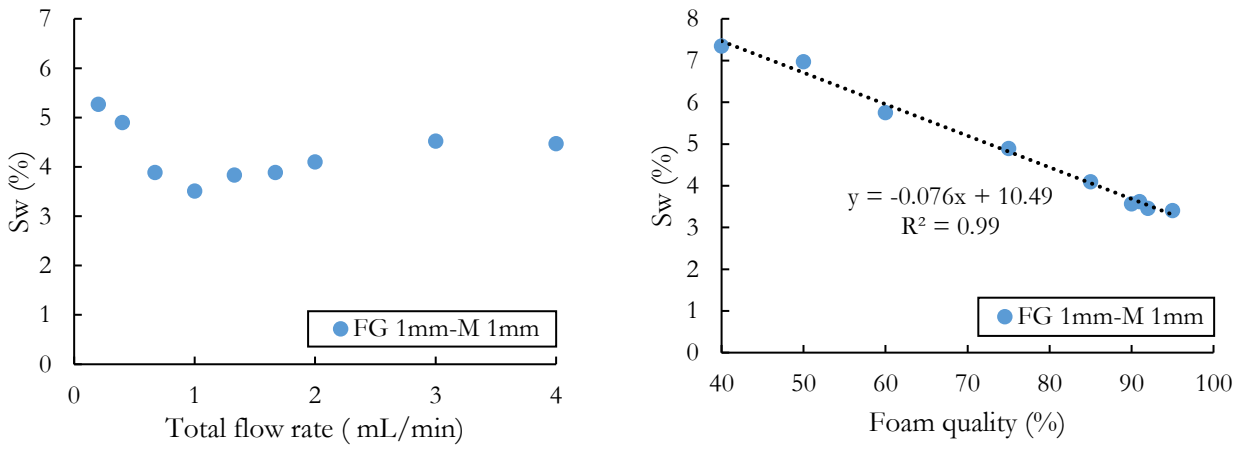

a) b)

Fig. 9 S_w as a function of a) total flow rate at fixed foam quality (f_g=85%), b) foam quality at Q_t=2 mL/min

We also observe that S_w is lower than the fraction of initially injected liquid. This phenomenon can be explained through Fig. 10, which plots effluent volume as a function of PV. The gas breakthrough occurred after injection of 1.44 PV of pre-generated foam, which corresponds to a change of slope in the figure (dashed line). This means that we recover 1.44 times more liquid than the initial volume in the pores of the main column. Since the liquid

phase is continuous and S_w in the main column is three times lower than the injected foam quality, we assume that the liquid phase flows faster during the foam formation in porous media, thereby decreasing the liquid saturation in the main column. When the foam was fully formed and stabilized, the change of effluent weight corresponded to the mass of the injected fluid. This phenomenon resembles the drainage effect of foam due to gravity, in which accumulation of liquid can be observed on the bottom.

On the other hand, from the equation of the trend of the first half of the curve, we observed that the effluent flow rate was 12% lower than Q_t, which can also be explained from the compressibility of gas volume. Thus, the compressibility of gas delayed the breakthrough time. However, it should be noted that the cumulated effluent volume was 224.3 mL when the breakthrough occurred, elevating the main column PV to 18.5%. Consequently, the liquid saturation in high permeability porous media is much lower and depends on the flow rate, compared with porous media with low permeability.

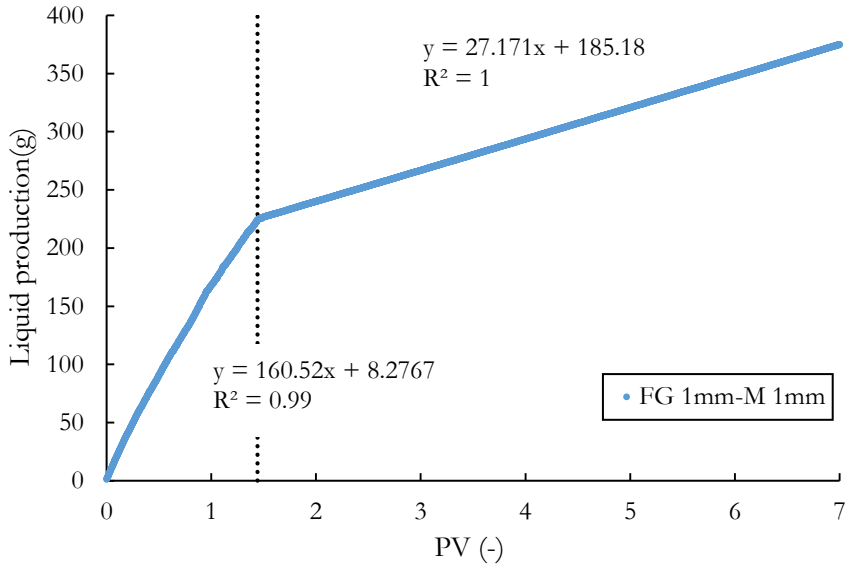

Fig. 10 Liquid volume of effluent as a function of PV for the 1 mm GB packed pre-generator and the main column at Q_t=3 mL/min (f_g=85%)

5.2 Effect of foam quality on foam flow behavior

We determined the transition foam quality between low-quality and high-quality regimes in order to select the unique foam quality for further investigation of the rheology of foam.

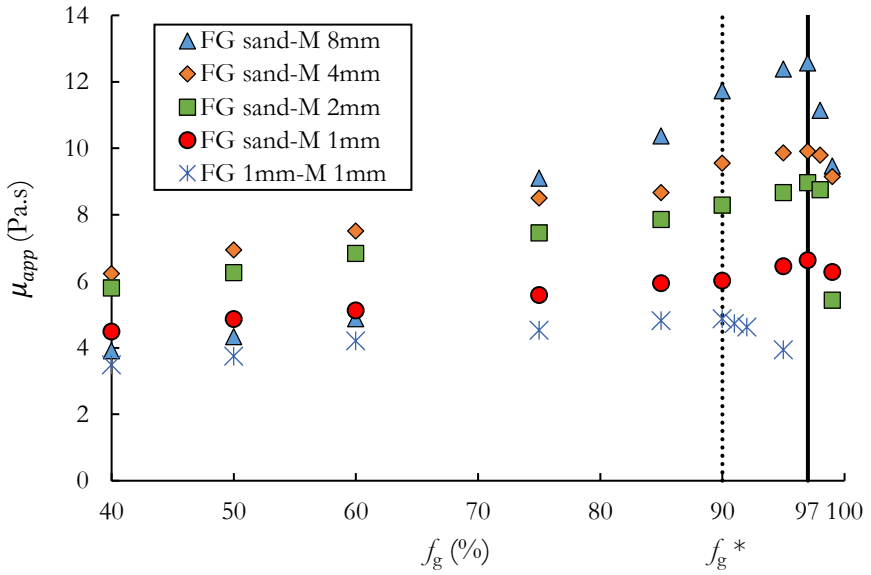

Fig. 11 Apparent foam viscosity as a function of foam quality at the fixed total flow rate (Q_t=2 mL/min)

Fig. 11 shows the change of the apparent foam viscosity calculated using Darcy's law as a function of foam quality. In this figure, the colored dots represent the results of foam generated by the sand-filled foam generator, and star dots are the result of the foam made through the 1 mm glass beads generator. By comparison of the results for foam generated by the sand column, we see that the apparent viscosity of foam is roughly proportional to the size of the grain diameter. The vertical lines spot the transition foam quality f_g^*, which is the limit between low-quality and high-quality regimes. The transition foam quality (f_g^*) is 97% for all glass beads, and is independent of the grain size (and porous medium permeability). As we observed in the Fig. 11, the apparent viscosity of the foams increases with the foam quality up to the f_g^*. Osei-Bonsu et al. (*34*) also found an increase in the apparent foam viscosity with the foam quality through the Hele-Shaw cell. However, they did not notice f_g^* even when f_g=99%, which showed the nature of the bulk foam. Alvarez et al. (*17*) showed a high f_g^* value (97%) for a foam generated through bronze wool in a high-permeability medium. By highly permeable medium, they insinuated sandpack with a permeability of 3.1 Darcy. They demonstrated that the f_g^* increases with permeability by taking into account the hypothesis that the bubble size is fixed at the low-quality regime (*21*). Lower capillary pressures in bigger pores accompanied the idea of high values of f_g^*, hence showed a much higher f_g^* in the sandpack.

In a low-quality regime, the results are consistent with the model of Rossen and Wang (*21*), where the bubble size is fixed, and the apparent viscosity only depends on the porous medium's structure and on surface tension. However, the decrease of apparent viscosity for foam quality lower than 75% for 8 mm GB can be explained by the transition of foam to the state of bubbly liquid (*67*).

On the contrary, foam generated using 1 mm GB and injected into the same porous medium has a lower transition foam quality (90%), which could be explained by the difference in bubble size of pre-generated foams. As previously mentioned, the mean bubble size generated in the sand is smaller than the pore size of the glass beads. Therefore, if the equivalent pore size is larger than the equivalent bubble size, the foam can behave as bulk foam. These circumstances are close to the foam flow in fractures, where the f_g^* for the limiting capillary pressure was

predicted to be as high as 99.95% (*68*). Consequently, we can conclude that f_g^* depends significantly on bubble size (structure of the foam generator).

5.3 Effect of foam bubble size on foam rheology

In Fig. 12, the results of apparent viscosity as a function of flow rate are compared in 1 mm GB main column, in which foam was pre-generated in the sand (circular points) and 1 mm glass beads (star points). Fig. 12 shows non-Newtonian, shear-thinning behavior of foam flow for the foam pre-generated in the sand column. With low flow rates, the apparent viscosity of foam generated by 1 mm glass beads is much smaller than the viscosity for foam made by sand.

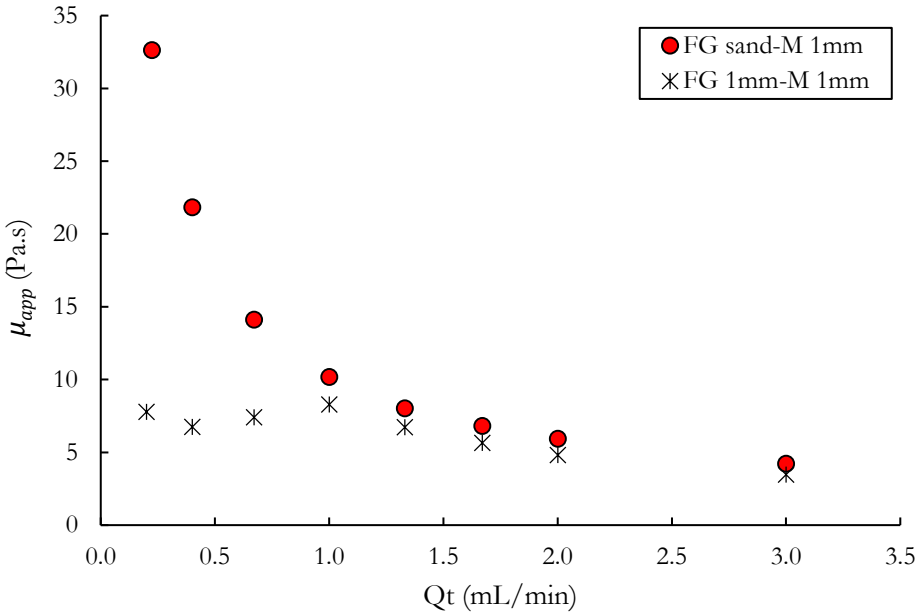

Fig. 12 Apparent viscosity of foam versus total flow rate in 1 mm glass bead main column (f_g=85 %)

We observe linear variation for apparent viscosity at low flow rates and a gradual transition to shear-thinning behavior when the flow rates are increased (1 mL/min and above) for the foam generated through the FG 1 mm. This behavior is similar to the study of Vassenden and Holt (*16*), in which they demonstrated a model for Newtonian behavior of foam flow at low flow rates and transition to shear-thinning behavior while increasing flow rate. However, their investigation was based on the study of Falls et al. (*5*), in which the existence of yield pressure drop stops lamellae flow if the pressure gradient is insufficient to move them, so they demonstrated the transition from Newtonian to shear-thinning behavior by a change from the limiting capillary pressure (*69*) to the limiting pressure gradient regime by increasing the rate.

First, for foam formed in the FG 1 mm, we assumed at that this state the foam flow was related to the yield stress: when the flow needs a particular pressure gradient to move out. This phenomenon was also observed during the experiments. At low flow rates, the effluent flow was stopped and resumed with a specific sequence in order to obtain a particular strength to withstand the yield stress. Second, the foam produced through the sand generator had smaller bubbles than pores of a 1 mm GB pack (bulk foam behavior). This means that no foam generation and destruction occurs, except coalescence, the coarsening of bubbles due to the gas diffusion from small to big

bubbles (Ostwald ripening, (*70*)). However, for foam that is pre-generated and injected in 1 mm GB columns, foam generation and destruction processes could also take place since the bubble size is assumed to be roughly the same size as the pore.

Fig. 13 shows the values of N_{cL} as a function of the flow rate, which is calculated using Eq. 1. The capillary number increased with the flow rate and was higher for foam generated in the sand. The changing trend of the foam data produced with 1 mm GB had a particular shift in the region of 1 mL/min. The transition zone between weak and strong foams explains this.

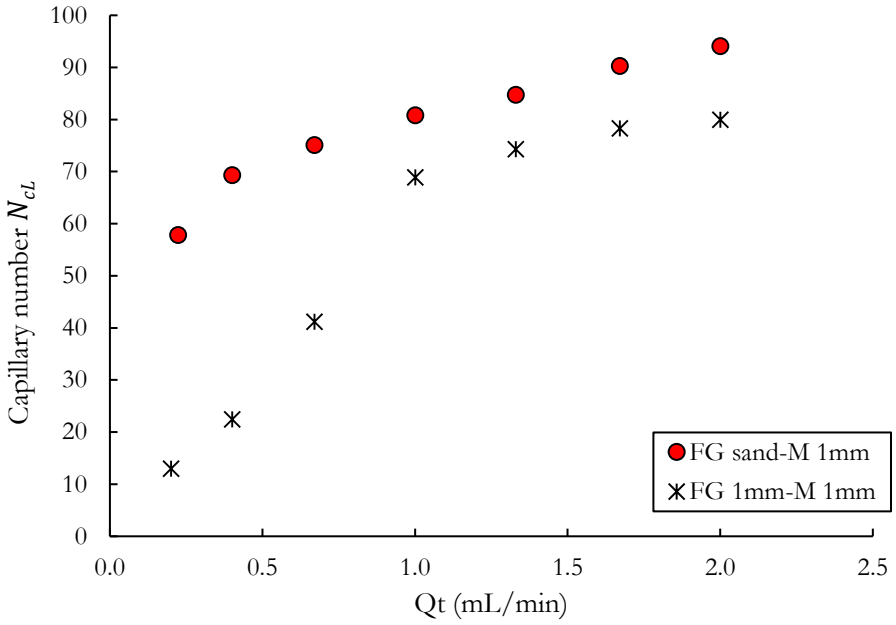

Fig. 13 Capillary number as a function of flow rates in 1 mm GB main column

Consequently, these results can also be explained by foam-generation processes, which depend on the flow rate or pressure drop. As shown in Fig. 1, strong foam formation occurs at the particular pressure drop, despite the minimum ∇P^*. A specific transition zone exists in terms of ∇P between the generation of weak and strong foams.

5.4 Effect of grain size (permeability) on foam rheology

In Fig. 14, the apparent viscosity as a function of the total flow rate are plotted for all GB sizes. The apparent foam viscosity in porous media increases with the size of grain diameter and decreases when the flow rate increases. Therefore, shear-thinning foam-flow behavior can be observed. To investigate the foam rheology, the apparent viscosity (μ_{app}) results were considered in terms of the equivalent shear rate ($\dot{\gamma}_{eq}$) using the following equation (*71*):

$$\dot{\gamma}_{eq} = \frac{4u/\varphi}{r_p} \tag{8}$$

where u (m/s) is the superficial velocity of the fluid (foam) in the porous columns.

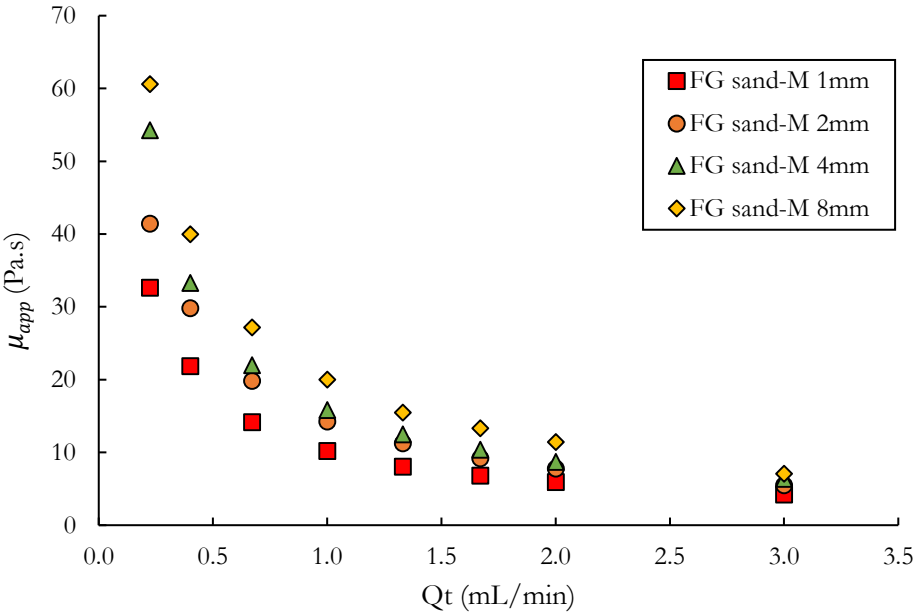

Fig. 14 Apparent viscosity versus total flow rate for d=1, 2, 4 and 8 mm glass beads using sand foam generator (f_g=85%)

From Eq. 8 and considering the variations of permeability (K) with the pore size (r_p) and porosity (φ) given in Table 1, it is evident that the shear rate becomes lower when porous media permeability increases for a particular flow rate value.

Fig. 15 shows the apparent viscosity results with fitting curves versus the equivalent shear rate. Contrary to Fig. 14, for a constant shear rate, the μ_{app} of foam decreases with increasing grain size (permeability). As the same foam was studied with different sizes of glass bead packings made with identical material, the only distinction between the main columns was grain size, consequently, pore size. This phenomenon can be attributed to the ratio of bubble size to pore size. For instance, if we assume that foam bubble size of foam is roughly equal to the pore size of the foam generator and that it is fixed during the experiment, the number of bubbles in the pore of 1 mm, 2 mm, 4 mm and 8 mm GB packings will be equal to 11, 22, 40 and 77, respectively. Consequently, friction between bubbles and porous media geometry decreases with increasing bubble numbers per pore.

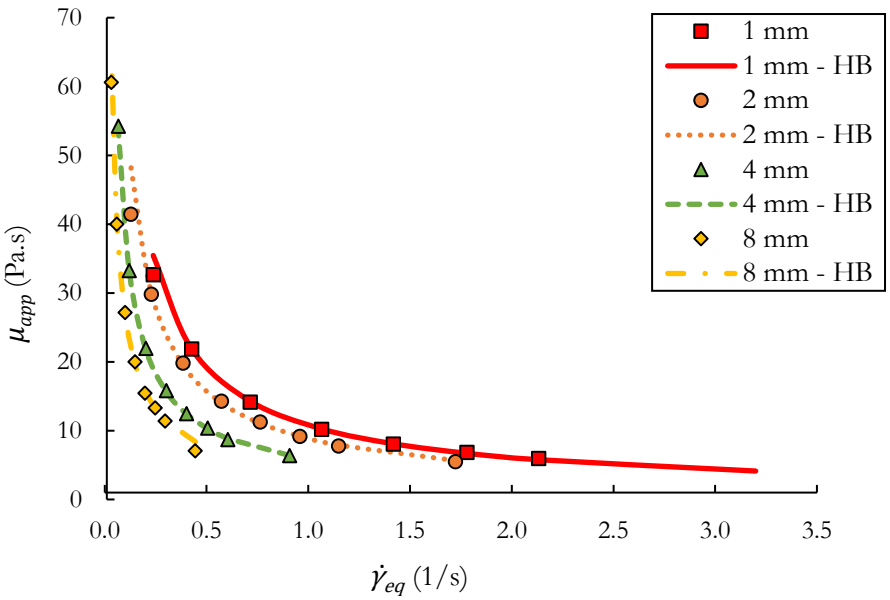

Fig. 15 Apparent viscosity as a function of shear rate for d=1, 2, 4 and 8 mm GB and sand foam generator

As can be seen, the experimental results fit the Herschel-Bulkley model very well (Eq. 4). The corresponding fitting values for glass beads are listed in Table 4.

Table 4 Fitting parameters for H-B model

Grain size diameter (mm)	1 mm	2 mm	4 mm	8 mm
n (-)	0.68	0.66	0.54	0.39
τ_0 (Pa)	7.72	5.83	3.09	1.44
k (kg/m.s)	2.96	2.97	3.00	3.00
R^2	0.99	0.95	0.99	0.99

The results presented in Table 4 show that foam is a yield-stress fluid and that yield stress values, $\tau_{0,}$ decrease with increasing grain size (permeability). The yield stress fluid index n is less than one, which indicates that in the conditions of our experiments, foam has a shear-thinning fluid behavior. We also observe that n decreases with increasing glass bead size.

6. Conclusions

This work presents a study of foam flow in high permeability porous media. Column experiments were conducted to study the behavior of pre-generated foam in high permeability porous media. Foam generation in packed fine sand and 1 mm glass beads were analyzed to study the effect of bubble size on the apparent foam viscosity. The impact of foam quality on the apparent foam viscosity, with a fixed flow rate, was examined to distinguish low and high-quality regimes. The rheology of foam with 85% foam quality was studied for different glass beads sizes. We drew the following conclusions:

- The foam generator plays a crucial role in foam displacement in porous media. Indeed, the pre-generation of foam in a less permeable column than the main column strengthens the apparent foam viscosity and

foam stability. This phenomenon may contribute to the bubble size since the viscosity is higher for a foam containing smaller gas bubbles.

- The liquid saturation in high permeability porous media is much lower and depends on the flow rate compared to porous media with low permeability.
- Foam generated in packed fine sand has a higher foam quality transition value than foam generated in packed glass beads. However, identical foam quality transition values were obtained for all glass bead sizes for foam generated through fine sand packing. Transition foam quality was, therefore, independent of the porous medium's permeability for highly permeable porous media when the bubbles were smaller than the pores. The transition foam quality was lower for foam flow with equivalent bubble and pore size.
- Foam in high permeability porous media was found to behave as a yield stress shear-thinning fluid regardless of porous medium grain size. The rheological behavior of foam is well fitted with the Herschel-Bulkley model. It was also shown that the apparent foam viscosity in GB packings (main column) increased with the diameter of the glass beads used to pack the main column for a given total flow rate. Hence, we propose considering foam as a yield stress fluid in highly permeable porous media where foam bubbles are much smaller than pores. When the bubbles are the same size as the pores, the foam behaves like a Newtonian fluid at low flow rates and exhibits a shear-thinning fluid behavior by increasing flow rates.

These insights can guide the study of pre-generated foam in highly permeable porous media, especially for application in soil remediation processes. We expect our study to be a starting point for further investigations on foam flow in high permeability porous media.

7. Acknowledgments

This study was performed as part of the "FAMOUS" project. The authors would like to thank ADEME for co-funding the project under the "GESIPOL" program and Bolashak International Scholarship from Kazakhstan government for providing the PhD grant for Sagyn Omirbekov. We gratefully acknowledge the financial support provided to the PIVOTS project by the "Région Centre – Val de Loire" and the European Regional Development Fund.

8. References

1. Hirasaki, G. J.; Miller, C. A.; Szafranski, R.; Lawson, J. B.; Akiya, N. Surfactant/Foam Process for Aquifer Remediation. *Society of Petroleum Engineers* **1997**.

2. Mulligan, C. N.; Eftekhari, F. Remediation with surfactant foam of PCP-contaminated soil. *Engineering Geology* **2003,** *70,* 269-279, Third British Geotechnical Society Geoenvironmental Engineering Conference.

3. Raza, S. H.; Marsden, S. S. The streaming potential and the rheology of foam. *Society of Petroleum Engineers Journal* **1967,** *7,* 359-368.

4. Hirasaki, G. J.; Lawson, J. B. Mechanisms of Foam Flow in Porous Media: Apparent Viscosity in Smooth Capillaries. *Society of Petroleum Engineers* **1985**.

5. Falls, A. H.; Musters, J. J.; Ratulowski, J. The apparent viscosity of foams in homogeneous bead packs. *SPE (Society of Petroleum Engineers) Reserv. Eng.; (United States)* **1989,** *4:2*.

6. Rossen, W. R.; Gauglitz, P. A. Percolation theory of creation and mobilization of foams in porous media. *AIChE Journal* **1990,** *36,* 1176-1188.

7. Dicksen, T.; Hirasaki, G. J.; Miller, C. A. Conditions for Foam Generation in Homogeneous Porous Media. *Society of Petroleum Engineers* **2002**.

8. Ransohoff, T. C.; Radke, C. J. Mechanisms of Foam Generation in Glass-Bead Packs. *Society of Petroleum Engineers* **1988**.

9. Gauglitz, P. A.; Friedmann, F.; Kam, S. I.; Rossen, W. R. Foam generation in homogeneous porous media. *Chemical Engineering Science* **2002,** *57,* 4037-4052.

10. Persoff, P.; Radke, C. J.; Pruess, K.; Benson, S. M.; Witherspoon, P. A. A laboratory investigation of foam flow in sandstone at elevated pressure. *SPE California Regional Meeting*, 1989.

11. Rossen, W. R. Rheology of foam in porous media at the" limiting capillary pressure. *IOR 1991-6th European Symposium on Improved Oil Recovery*, 1991; pp cp--44.

12. Ettinger, R. A.; Radke, C. J. The influence of texture on steady foam flow in Berea sandstone. *SPE* **1989**.

13. Patzek, T. W.; Koinis, M. T. Kern River Steam-Foam Pilots. *Society of Petroleum Engineers* **1990**.

14. Alvarez, J. M. *Foam-Flow Behavior in Porous Media: Effects of Flow Regime and Porous-Medium Heterogeneity;* Ph.D. dissertation; The University of Texas at Austin, 1998.

15. Bingham, E. C. Plastic flow. *Journal of the Franklin Institute* **1916,** *181,* 845-848.

16. Vassenden, F.; Holt, T. Experimental Foundation for Relative Permeability Modeling of Foam. *Society of Petroleum Engineers* **2000**.

17. Alvarez, J. M.; Rivas, H. J.; Rossen, W. R. Unified Model for Steady-State Foam Behavior at High and Low Foam Qualities. *Society of Petroleum Engineers* **2001**.

18. Rossen, W. R. Minimum pressure gradient for foam flow in porous media: Effect of interactions with stationary lamellae. *Journal of Colloid and Interface Science* **1990,** *139,* 457-468.

19. Cohen, D.; Patzek, T. W.; Radke, C. J. Onset of Mobilization and the Fraction of Trapped Foam in Porous Media. *Transport in Porous Media* **1997,** *28,* 253-284.

20. Nguyen, Q. P.; Currie, P. K.; Zitha, P. L. J. Motion of foam films in diverging–converging channels. *Journal of Colloid and Interface Science* **2004,** *271,* 473-484.

21. Rossen, W. R.; Wang, M. W. Modeling Foams for Acid Diversion. *Society of Petroleum Engineers* **1999**.

22. Balan, H. O.; Balhoff, M. T.; Nguyen, Q. P. Modeling of Gas Trapping and Mobility in Foam Enhanced Oil Recovery. *Energy Fuels* **2011,** *25 (9),* 3974-3987.

23. Zitha, P. L. J.; Du, D. X. A new stochastic bubble population model for foam flow in porous media. *Transport in Porous Media* **2010,** *83,* 603-621.

24. Simjoo, M.; Nguyen, Q. P.; Zitha, P. L. J. Rheological Transition during Foam Flow in Porous Media. *Industrial & Engineering Chemistry Research* **2012**.

25. Simjoo, M.; Zitha, P. L. J. Modeling and Experimental Validation of Rheological Transition During Foam Flow in Porous Media. *Transport in Porous Media* **2020,** *131,* 315-332.

26. Chen, M.; Yortsos, Y. C.; Rossen, W. R. Insights on foam generation in porous media from pore-network studies. *Colloids and Surfaces A: Physicochemical and Engineering Aspects* **2005,** *256,* 181-189.

27. Friedmann, F.; Chen, W. H.; Gauglitz, P. A. Experimental and simulation study of high-temperature foam displacement in porous media. *SPE (Society of Petroleum Engineers) Reservoir Engineering; (United States)* **1991,** *6:1*.

28. Kovscek, A. R.; Tadeusz, W. P.; Radke, C. J. Mechanistic foam flow simulation in heterogeneous and multidimensional porous media. *SPE Journal* **1997,** *2,* 511-526.

29. Bertin, H. J.; Quintard, M. Y.; Castanier, L. M. Development of a Bubble-Population Correlation for Foam-Flow Modeling in Porous Media. *Society of Petroleum Engineers* **1998**.

30. Myers, T. J.; Radke, C. J. Transient Foam Displacement in the Presence of Residual Oil: Experiment and Simulation Using a Population-Balance Model. *Industrial & Engineering Chemistry Research* **2000**.

31. Kam, S. I. Improved mechanistic foam simulation with foam catastrophe theory. *Colloids and Surfaces A: Physicochemical and Engineering Aspects* **2008,** *318,* 62-77.

32. Kovscek, A. R.; Chen, Q.; Gerritsen, M. Modeling Foam Displacement With the Local-Equilibrium Approximation: Theory and Experimental Verification. *Society of Petroleum Engineers* **2010**.

33. Ashoori, E.; Marchesin, D.; Rossen, W. R. Multiple Foam States and Long-Distance Foam Propagation in EOR Displacements. *Society of Petroleum Engineers* **2012**.

34. Osei-Bonsu, K.; Shokri, N.; Grassia, P. Fundamental investigation of foam flow in a liquid-filled Hele-Shaw cell. *Journal of colloid and interface science* **2016,** *462,* 288-296.

35. Osterloh, W. T.; Jante Jr, M. J. Effects of gas and liquid velocity on steady-state foam flow at high temperature. *SPE/DOE Enhanced Oil Recovery Symposium*, 1992.

36. Shojaei, M. J.; Castro, A. R.; Méheust, Y.; Shokri, N. Dynamics of foam flow in a rock fracture: Effects of aperture variation on apparent shear viscosity and bubble morphology. *Journal of colloid and interface science* **2019,** *552,* 464-475.

37. Kovscek, A. R.; Radke, C. J. Fundamentals of foam transport in porous media. *ACS Advances in Chemistry Series* **1994,** *242,* 115-164.

38. Rossen, W. R. Theory of mobilization pressure gradient of flowing foams in porous media: I. Incompressible foam. *Journal of Colloid and Interface Science* **1990,** *136,* 1-16.

39. Drenckhan, W.; Saint-Jalmes, A. The science of foaming. *Advances in Colloid and Interface Science* **2015,** *222,* 228-259, Reinhard Miller, Honorary Issue.

40. Tanzil, D.; Hirasaki, G. J.; Miller, C. A. Mobility of foam in heterogeneous media: Flow parallel and perpendicular to stratification. *SPE Annual Technical Conference and Exhibition*, 2000.

41. Langevin, D. Aqueous foams and foam films stabilised by surfactants. Gravity-free studies. *Comptes Rendus Mécanique* **2017,** *345,* 47-55, Basic and applied researches in microgravity – A tribute to Bernard Zappoli's contribution.

42. Herschel, W. H.; Bulkley, R. Konsistenzmessungen von gummi-benzollösungen. *Colloid & Polymer Science* **1926,** *39,* 291-300.

43. Mao, X.; Jiang, R.; Xiao, W.; Yu, J. Use of surfactants for the remediation of contaminated soils: A review. *Journal of Hazardous Materials* **2015,** *285,* 419-435.

44. Tuvell, M. E.; Kuehnhanss, G. O.; Heidebrecht, G. D.; Hu, P. C.; Zielinski, A. D. AOS --- An anionic surfactant system: Its manufacture, composition, properties, and potential application. *Journal of the American Oil Chemists' Society* **1978,** *55,* 70-80.

45. Talmage, S. S. *Environmental and human safety of major surfactants: alcohol ethoxylates and alkylphenol ethoxylates;* CRC Press, 1994.

46. Arndt, R. *Alkyl Sulfonates and Alpha-Olefin Sulfonates: SIDS Initial Assessment Report;* Tech. rep.; BMU (Bundesministerium fur Umwelt, Naturschutz und Reaktorsicherheit), 2007.

47. Cserháti, T.; Forgács, E.; Oros, G. Biological activity and environmental impact of anionic surfactants. *Environment International* **2002,** *28,* 337-348.

48. Svab, M.; Kubal, M.; Müllerova, M.; Raschman, R. Soil flushing by surfactant solution: Pilot-scale demonstration of complete technology. *Journal of Hazardous Materials* **2009,** *163,* 410-417.

49. Stauffer, C. E. The measurement of surface tension by the pendant drop technique. *The journal of physical chemistry* **1965,** *69,* 1933-1938.

50. Yoon, I.-H.; Yoon, S. B.; Jung, C.-H.; Kim, C.; Kim, S.; Moon, J.-K.; Choi, W.-K. A highly efficient decontamination foam stabilized by well-dispersed mesoporous silica nanoparticles. *Colloids and Surfaces A: Physicochemical and Engineering Aspects* **2019,** *560,* 164-170.

51. Simjoo, M.; Rezaei, T.; Andrianov, A.; Zitha, P. L. J. Foam stability in the presence of oil: effect of surfactant concentration and oil type. *Colloids and Surfaces A: Physicochemical and Engineering Aspects* **2013,** *438,* 148-158.

52. Belhaij, A.; AlQuraishi, A.; Al-Mahdy, O. Foamability and foam stability of several surfactants solutions: the role of screening and flooding. *SPE Saudi Arabia Section Technical Symposium and Exhibition*, 2014.

53. Verma, A.; Chauhan, G.; Ojha, K. Characterization of α-olefin sulfonate foam in presence of cosurfactants: Stability, foamability and drainage kinetic study. *Journal of Molecular Liquids* **2018,** *264,* 458-469.

54. Farzaneh, S. A.; Sohrabi, M. Experimental investigation of CO2-foam stability improvement by alkaline in the presence of crude oil. *Chemical Engineering Research and Design* **2015,** *94,* 375-389.

55. Tan, S. N.; Fornasiero, D.; Sedev, R.; Ralston, J. The role of surfactant structure on foam behaviour. *Colloids and Surfaces A: Physicochemical and Engineering Aspects* **2005,** *263,* 233-238.

56. Dong, X.; Xu, J.; Cao, C.; Sun, D.; Jiang, X. Aqueous foam stabilized by hydrophobically modified silica particles and liquid paraffin droplets. *Colloids and Surfaces A: Physicochemical and Engineering Aspects* **2010,** *353,* 181-188.

57. Wang, J.; Liu, H.; Ning, Z.; Zhang, H. Experimental research and quantitative characterization of nitrogen foam blocking characteristics. *Energy & Fuels* **2012,** *26,* 5152-5163.

58. Paria, S. Surfactant-enhanced remediation of organic contaminated soil and water. *Advances in Colloid and Interface Science* **2008,** *138,* 24-58.

59. Sander, R. *Compilation of Henry's law constants for inorganic and organic species of potential importance in environmental chemistry;* Max-Planck Institute of Chemistry, Air Chemistry Department Mainz, Germany, 1999.

60. Farajzadeh, R.; Andrianov, A.; Bruining, H.; Zitha, P. L. J. Comparative Study of CO2 and N2 Foams in Porous Media at Low and High Pressure−Temperatures. *Industrial & Engineering Chemistry Research* **2009,** *48,* 4542-4552.

61. Darcy, H. P. G. *Les Fontaines publiques de la ville de Dijon. Exposition et application des principes à suivre et des formules à employer dans les questions de distribution d'eau, etc;* V. Dalamont, 1856.

62. Kozeny, J. Uber kapillare leitung der wasser in boden. *Royal Academy of Science, Vienna, Proc. Class I* **1927,** *136,* 271-306.

63. Sutera, S. P.; Skalak, R. The history of Poiseuille's law. *Annual review of fluid mechanics* **1993,** *25,* 1-20.

64. Falls, A. H.; Hirasaki, G. J.; Patzek, T. W.; Gauglitz, D. A.; Miller, D. D.; Ratulowski. Development of a Mechanistic Foam Simulator: The Population Balance and Generation by Snap-Off. *Society of Petroleum Engineers* **1988**.

65. Roof, J. G. Snap-off of oil droplets in water-wet pores. *Society of Petroleum Engineers Journal* **1970,** *10,* 85-90.

66. Ma, K.; Liontas, R.; Conn, C. A.; Hirasaki, G. J.; Biswal, S. L. Visualization of improved sweep with foam in heterogeneous porous media using microfluidics. *Soft Matter* **2012,** *8,* 10669-10675.

67. Ramadan, A.; Kuru, E.; Saasen, A. Critcal Review of Drilling Foam Rheology. *ANNUAL TRANSACTIONS-NORDIC RHEOLOGY SOCIETY* **2003,** *11,* 63-72.

68. Pancharoen, M.; Fernø, M. A.; Kovscek, A. R. Modeling foam displacement in fractures. *Journal of Petroleum Science and Engineering* **2012,** *100,* 50-58.

69. Khatib, Z. I.; Hirasaki, G. J.; Falls, A. H. Effects of capillary pressure on coalescence and phase mobilities in foams flowing through porous media. *SPE reservoir engineering* **1988,** *3,* 919-926.

70. Voorhees, P. W. The theory of Ostwald ripening. *Journal of Statistical Physics* **1985,** *38,* 231-252.

71. Darby, R.; Darby, R.; Chhabra, R. P. *Chemical engineering fluid mechanics, revised and expanded;* CRC Press, 2001.